# Short Papers

## Matched Windows in Circular Waveguide

LAWRENCE CARIN, KEVIN J. WEBB, MEMBER, IEEE, AND SANDER WEINREB, FELLOW, IEEE

*Abstract*—**Design curves are presented for the matching of a dielectric window in circular waveguide propagating the dominant $TE_{11}$ mode. The matching is accomplished by thick or thin inductive irises which are in contact with the window on both sides. This configuration gives wide bandwidth and is mechanically convenient, but requires consideration of coupling of the higher order modes generated by the closely spaced discontinuities. Mode matching and the generalized scattering matrix are utilized.**

### I. Introduction

Dielectric windows are often required to separate one gas from another or to provide a vacuum in a waveguide system. The particular application which prompted this investigation was the circular waveguide connection of a dual, linearly polarized feed horn, pressurized with dry nitrogen, to a low-noise receiver which is cryogenically cooled and therefore must be in high vacuum.

To a first approximation the window presents a capacitive discontinuity across the equivalent transmission line and therefore an inductive iris to parallel resonate the capacitor is suggested. Greater bandwidth should result if an iris is used on each side of the dielectric. The resulting cross section is shown in Fig. 1, where the five parameters ($d$, $d_i$, $t$, $t_i$, and $\epsilon_r$) are defined. The two irises form a convenient mechanical design for mounting and sealing the window; the iris on one side is machined into the waveguide wall while the iris on the other side is in the form of a ring. Fine tuning of the frequency of best match can then be achieved by changing the inner diameter of the ring.

The waveguide system of Fig. 1 will be analyzed using mode matching [1]–[6] to find the modes excited by each of the four step discontinuities. The fields excited at each discontinuity can be expressed in the form of a generalized scattering matrix [4]–[7]. For the first discontinuity only the dominant $TE_{11}$ mode is incident while for subsequent discontinuities a number, $N$, of higher order modes (some of which may be propagating depending on $\epsilon_r$) are considered; $N$ must be carefully chosen to give sufficient accuracy and maintain reasonable computation time. The series of discontinuities is treated by cascading the generalized scattering matrices [4]–[7] of the individual junctions to obtain a generalized scattering matrix for the entire system.

In the next section the results of our analysis are presented in a way useful for the design of matched windows in circular waveguides propagating the $TE_{11}$ mode. This is followed by a summary of the analysis method and some checks of its validity. A complete description of the analysis method is given in the thesis of Carin [6].

Manuscript received December 5, 1987; revised March 29, 1988.

L. Carin and K. J. Webb are with the Department of Electrical Engineering, University of Maryland, College Park, MD 20742.

S. Weinreb is with the National Radio Astronomy Observatory, Charlottesville, VA 22903.

IEEE Log Number 8822327.

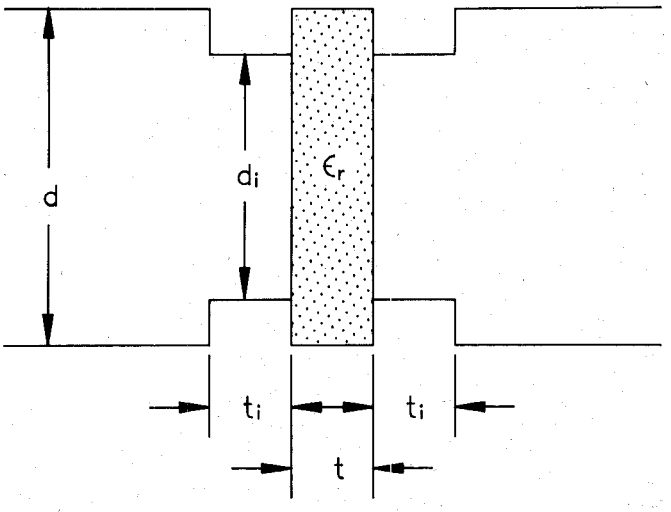


Fig. 1. Cross-sectional view of a circular waveguide dielectric window. The waveguide has diameter $d$, the iris has diameter $d_i$ and thickness $t_i$, and the window has dielectric constant $\epsilon_r$ and thickness $t$.

### II. Results

The two design questions which we attempt to answer in Figs. 2 and 3 are the following:

1) What is the optimum iris inner diameter given the window thickness, dielectric constant, iris thickness, waveguide diameter, and operating frequency?
2) Given an iris optimized for a given frequency, what is the frequency response of the window?

The optimum iris diameter was defined to be that dimension which produced the smallest reflection coefficient (lowest insertion loss) for a given set of parameters. The optimization was achieved using the subroutine ZXGSP from the IMSL Problem Solving Software System (1985). The designer is not just interested in low insertion loss at a fixed frequency, but rather is also concerned about how the design will perform over the entire frequency band to be used (frequencies over which single moded operation is possible). For this reason, the frequency response of the window is presented for each geometry that was initially optimized for a single frequency. The figure captions explain the design curves. To present the results in a compact manner, it is necessary to select two ratios of iris to window thickness. All dimensions are normalized to the waveguide diameter $d$, and frequency is normalized to the $TE_{11}$ mode cutoff frequency $f_c = 17.58/d$ where $f_c$ is in GHz and $d$ is in cm. The graphs were computed with a Fortran program on a VAX 11/785 computer. For a particular geometry and frequency, it required about 40 seconds of CPU time to calculate the scattering parameters for the series of step discontinuities in Fig. 1. To find the iris diameter for which the matching irises were optimal at a given frequency (Fig. 2), an average of 5 minutes of CPU time was required per point.

0018-9480/88/0900-1359$01.00 ©1988 IEEE

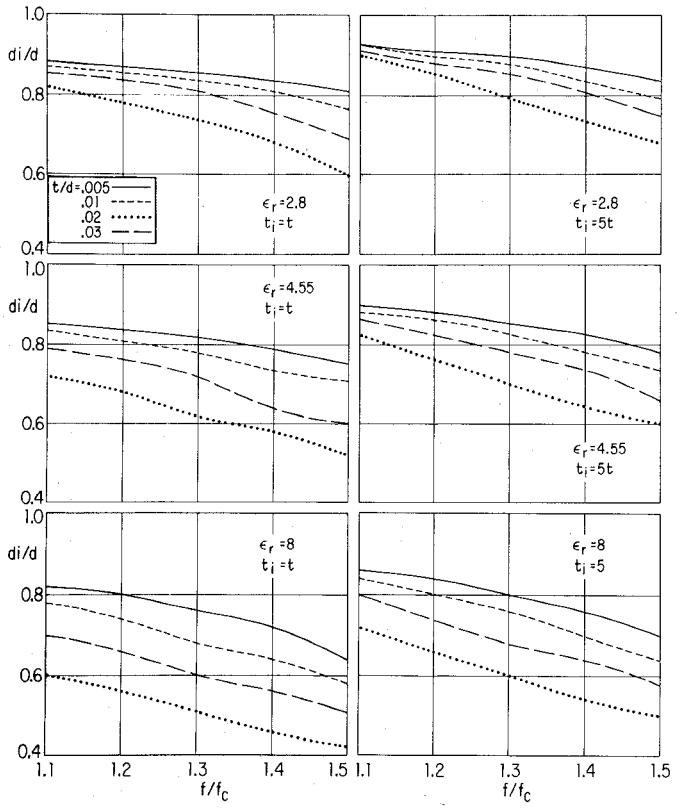


Fig. 2. Optimum iris diameter as a function of normalized frequency, $f/f_c$. In each graph the optimum normalized iris diameter, $d_i/d$, is plotted for four different values of normalized window thickness $t/d$. The left graphs are for iris thickness $t_i = t$, and the right graphs are for $t_i = 5t$, and from top to bottom the dielectric constants are 2.80 (Mylar), 4.55 (quartz), and 8.0 (glass).

## III. Mode Matching Formulation

Mode matching has been used extensively to analyze waveguide discontinuities [1]–[6]. The technique is reviewed here and key points relevant to this work are discussed. A generalized scattering matrix [4]–[7] is developed which handles an arbitrary number of propagating and evanescent modes incident from both sides of the discontinuity.

The transverse fields are expressed at the junction ($z = 0$) as a superposition of modes and the continuity of transverse electric and magnetic fields is applied:

$$\sum_{i=1}^{\infty} a_i^{(1)} \boldsymbol{e}_i^{(1)} + \sum_{i=1}^{\infty} b_i^{(1)} \boldsymbol{e}_i^{(1)} = \sum_{j=1}^{\infty} a_j^{(2)} \boldsymbol{e}_j^{(2)} + \sum_{j=1}^{\infty} b_j^{(2)} \boldsymbol{e}_j^{(2)} \quad (1)$$

and

$$\sum_{i=1}^{\infty} a_i^{(1)} Y_i^{(1)} \boldsymbol{h}_i^{(1)} - \sum_{i=1}^{\infty} b_i^{(1)} Y_i^{(1)} \boldsymbol{h}_i^{(1)} = -\sum_{j=1}^{\infty} a_j^{(2)} Y_j^{(2)} \boldsymbol{h}_j^{(2)} + \sum_{j=1}^{\infty} b_j^{(2)} Y_j^{(2)} \boldsymbol{h}_j^{(2)}. \quad (2)$$

The $\boldsymbol{e}_i^{(j)}$ and $\boldsymbol{h}_i^{(j)}$ are the normalized mode functions for the electric and magnetic fields, respectively, for mode $i$ in guide $j$. Guide 1 is to the left of the junction and guide 2 to the right of the junction. The coefficient $a_i^{(j)}$ represents the incident amplitude, and $b_i^{(j)}$, the excited (reflected) amplitude for mode $i$ in guide $j$. The wave admittance for mode $i$ in guide $j$ is denoted by $Y_i^{(j)}$. The waveguide cross sections in this paper are homogeneous so that the fields become a superposition of decoupled

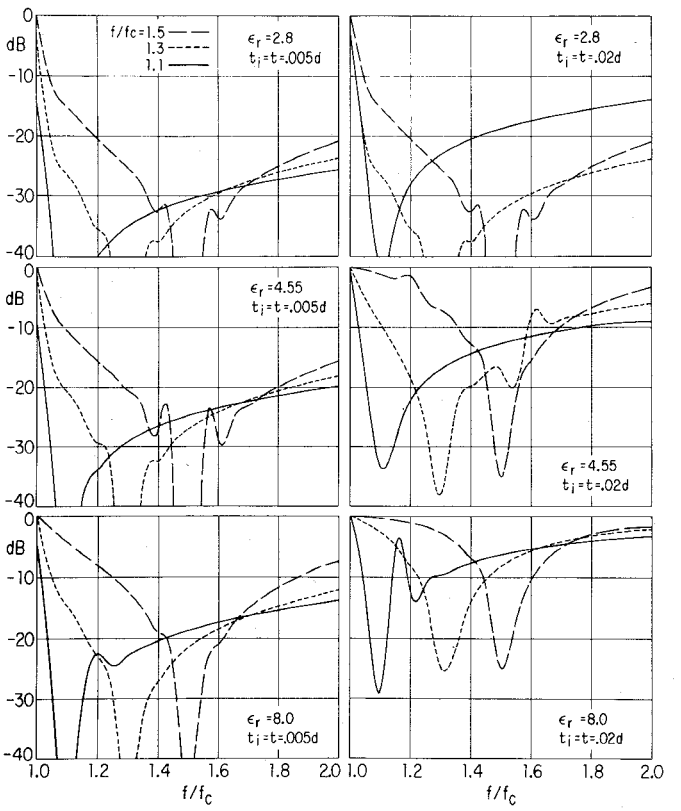


(a)

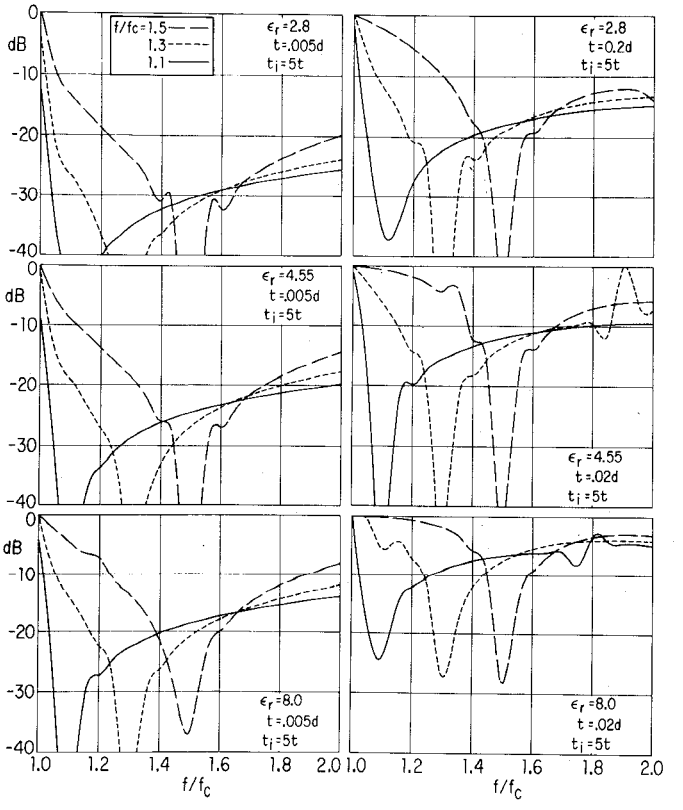


(b)

Fig. 3. (a) Each graph shows return loss, $20\log(|S_{11}|)$, as a function of normalized frequency for windows optimized for $f/f_c = 1.1$, 1.3, and 1.5. The left-hand graphs are for $t/d = 0.005$, and the right-hand graphs are for $t/d = 0.02$; from top to bottom the dielectric constants are 2.80, 4.55, and 8.0. For above results, $t_i = t$. (b) Same as (a) except for the thicker iris case, $t_i = 5t$.

transverse electric (TE) and transverse magnetic (TM) modes. In this case the wave admittance corresponds to either a TE or a TM mode. For the TE mode $Y_{TE} = k_z/\omega\mu$ and for the TM mode $Y_{TM} = \omega\epsilon/k_z$, where $k_z$ is the phase constant for the mode in the $z$ direction, and $\mu$ and $\epsilon$ are the permeability and the permittivity, respectively. Consider taking inner products with magnetic mode functions from guide 2 in (1) and with electric mode functions from guide 1 in (2). After truncating to $M$ modes in waveguide 1 and $N$ modes in waveguide 2, the result can be expressed in matrix form as

$$\underbrace{\left(\begin{array}{c|c} K_{p,l} & -\delta_{p,l} \\ p=1,\cdots,N & p=1,\cdots,N \\ l=1,\cdots,M & l=1,\cdots,N \\ \hline Y_p^{(1)}\delta_{p,l} & Y_l^{(2)}L_{p,l} \\ p=1,\cdots,M & p=1,\cdots,M \\ l=1,\cdots,M & l=1,\cdots,N \end{array}\right)}_{X_1} \underbrace{\left(\begin{array}{c} \cdot \\ \cdot \\ a_i^{(1)} \\ \cdot \\ \cdot \\ \hline \cdot \\ \cdot \\ a_j^{(2)} \\ \cdot \\ \cdot \end{array}\right)}_{a}$$

$$= \underbrace{\left(\begin{array}{c|c} -K_{p,l} & \delta_{p,l} \\ p=1,\cdots,N & p=1,\cdots,N \\ l=1,\cdots,M & l=1,\cdots,N \\ \hline Y_p^{(1)}\delta_{p,l} & Y_l^{(2)}L_{p,l} \\ p=1,\cdots,M & p=1,\cdots,M \\ l=1,\cdots,M & l=1,\cdots,N \end{array}\right)}_{X_2} \underbrace{\left(\begin{array}{c} \cdot \\ \cdot \\ b_i^{(1)} \\ \cdot \\ \cdot \\ \hline \cdot \\ \cdot \\ b_j^{(2)} \\ \cdot \\ \cdot \end{array}\right)}_{b} \tag{3}$$

where

$$K_{p,l} = \int_{S_1} \boldsymbol{e}_l^{(1)} \times \boldsymbol{h}_p^{(2)} \cdot d\boldsymbol{s}_1 \tag{4}$$

$$L_{p,l} = \int_{S_1} \boldsymbol{e}_p^{(1)} \times \boldsymbol{h}_l^{(2)} \cdot d\boldsymbol{s}_1 \tag{5}$$

and $i=1,\cdots,M$ and $j=1,\cdots,N$. The generalized scattering matrix of the step discontinuity is

$$S = \left(\begin{array}{c|c} S_{11} & S_{12} \\ \hline S_{21} & S_{22} \end{array}\right) = X_2^{-1} \cdot X_1 \tag{6}$$

where $S_{11}$, $S_{12}$, $S_{21}$, and $S_{22}$ are $M \times M$, $M \times N$, $N \times M$, and $N \times N$ matrices, respectively, and $X_1$ and $X_2$ are as defined in (3).

The above formulation is valid for any waveguide system for which there is a step discontinuity. This paper concentrates on step discontinuities in circular waveguide. The work is simplified by the fact that the mode functions for circular waveguide, as well as the inner products, can be expressed in closed form. The normalized mode functions for circular waveguide are found in the *Waveguide Handbook* [9] and the inner products are derived in Carin's thesis [6].

As described by Wexler [1], the solution of the step discontinuity converges fastest if the boundary reduction and enlargement are handled separately. We began by stating that the boundary conditions to be met at the discontinuity are the continuity of tangential electric and magnetic fields across the aperture, as well as the vanishing of the tangential electric field on the perfectly conducting obstacle (wall). When the tangential fields are matched as in (1) and (2), the first boundary condition has been enforced. To meet the last boundary condition care must be taken. For the case of boundary reduction, if magnetic mode functions from guide 2 are used to take inner products with (1), the inner products support exists only over the smaller guide's cross section. All the integrals are nonzero only over the aperture and not over the wall. In our study it was determined that this choice of testing functions yields very slow convergence for the boundary condition that the transverse electric field be zero on the conductor, in agreement with Wexler. To have some of the inner products with support over the junction wall, magnetic mode functions from the larger guide (guide 1 in this case) are used on the electric field continuity equation. The same argument holds for the selection of testing functions for the boundary enlargement case; i.e., magnetic mode functions from the larger guide (guide 2) are again used on the electric field continuity equation. Using the above discussion as a guideline, it is seen that (3), (4), and (5) correspond to a boundary enlargement discontinuity.

One might initially attempt to use transmission matrices to describe each step and then cascade these matrices to determine the total transmission matrix for the series of step discontinuities. This transmission matrix can then be converted to the more common scattering matrix. The problem with this approach is that for many geometries the exponential factor associated with the evanescent modes will lead to numbers that exceed the available numerical range of the computer. A method of cascading generalized scattering matrices that alleviates this problem has been developed by Chu and Itoh [7]. A composite scattering matrix is then generated that describes the series of steps.

The way in which the number of modes in the continuity equations of electric and magnetic fields ((1) and (2)) are truncated is often of importance. Assume $M$ modes in guide 1 (left of junction) and $N$ modes in guide 2 (right of junction) are retained in the summations. Investigations on the rate on convergence for different values of $M$ and $N$ have been reported by other authors [2]–[4]. Based on these results it is concluded that the convergence rate is improved when $M/N$ corresponds to the ratio of the cross-sectional areas of the waveguides on either side of the junction. In other words, for the circular waveguide considered here, $M/N = r_1^2/r_2^2$ (to the closest integer) with $r_1$ and $r_2$ the radii of guide 1 and 2, respectively. It was determined in our study of circular waveguides that the convergence rate of the reflection coefficient was not very sensitive to the ratio $(M/N)$ used in the field expansion as long as the number of modes, $M$ and $N$, were sufficiently large ($N = M = 10$). This is in agreement with English [3], who shows that the reflection coefficient converges sufficiently after ten modes for step sizes comparable to those considered in this paper. Although it was found that the reflection coefficient converged fastest when $M/N$ corresponded to the ratio suggested in the literature and stated above, it was not sufficiently faster to warrant using this ratio as opposed to simply using an equal number of modes ($M = N = 10$) on each side of the discontinuity. This was because the discontinuities encountered in this work were relatively small, but as the difference in cross-sectional area between the guides increases, the number of modes needed to express the fields in the larger guide increases. Thus, it becomes numerically efficient to optimize the ratio $M/N$ as the difference in the cross-sectional areas of the two guides increases so that fewer total modes will be needed in the field expansion.

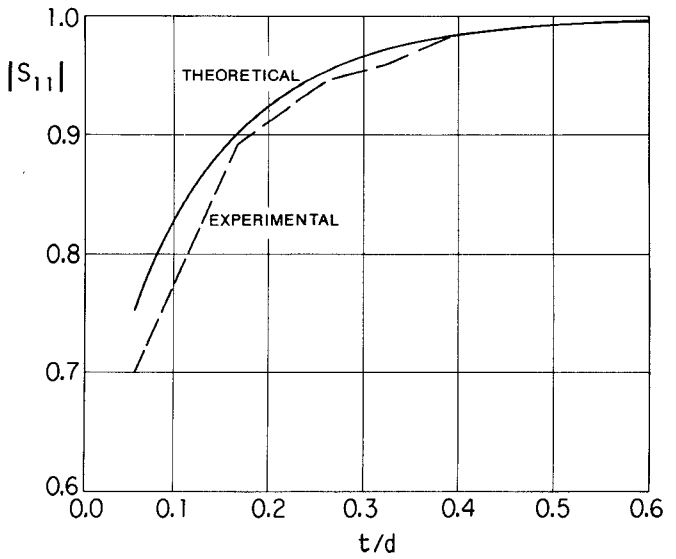


Fig. 4. Comparison of theoretical results of this paper with experimental results of Ragan [10] for a single, thick inductive iris with $d = 23.8$ mm, $d_t/d = 0.60$, and $f = 9.375$ GHz. The magnitude of the reflection coefficient is shown as a function of normalized iris thickness, $t/d$.

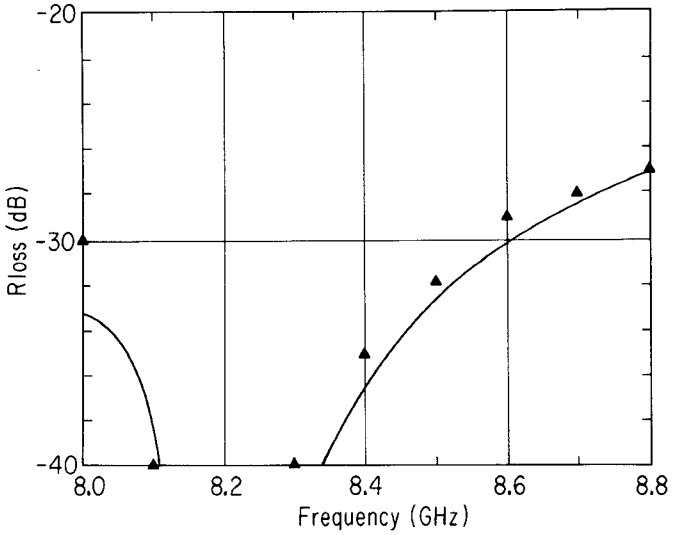


Fig. 5. Comparison of measured data with theory presented in this paper for a rexolite window with $d = 1.02$ in, $d_t = 0.855$ in, $t = 0.025$ in, and $t_t = 0.031$ in. The points represent the experiment, the curve, theory.

## IV. Verification of Theory

For the cascade of circular waveguide step discontinuities there is a scarcity of data with which to compare. Ragan [10] presents some experimental results for the inductive iris in a circular waveguide. Ragan gives an equivalent circuit model with parameter values obtained from experimental results. He makes a comparison between the experimental data and theory for small holes in an infinitesimally thin iris. The results show that this theory has severe limitations when the size of the hole becomes large relative to the iris thickness. The iris consists of two step discontinuities, from left to right, a diameter reduction and diameter enlargement, separated by a homogeneous circular waveguide. Using the theory of the previous section, the two steps are modeled with generalized scattering matrices and then cascaded using the transmission matrix of the interconnecting circular waveguide. The theoretical results, in the form of reflection coefficient, are found to be in excellent agreement with Ragan's experimental data, as shown in Fig. 4.

An experiment was carried out for a Rexolite ($\epsilon_r = 2.54$) window with $d = 1.02$ in, $d_t = 0.855$ in, $t = 0.025$ in, and $t_t = 0.031$ in. The theoretical results show good agreement with experimental results, as shown in Fig. 5.

## References

[1] A. Wexler, "Solution of waveguide discontinuities by modal analysis," *IEEE Trans Microwave Theory Tech.*, vol. MTT-15, pp. 508–517, Sept. 1967

[2] P. H Masterman and P. J. B. Clarricoats, "Computer field-matching of waveguide transverse discontinuities," *Proc. Inst Elec. Eng*, vol 118, no. 1, pp 51–63, Jan. 1971

[3] W. J. English, "The circular waveguide step-discontinuity mode transducer," *IEEE Trans. Microwave Theory Tech*, vol MTT-21, pp. 633–636, Oct. 1973.

[4] G. L. James, "Admittance of irises in coaxial and circular waveguides for $TE_{11}$-mode excitation," *IEEE Trans Microwave Theory Tech*, vol MTT-35, pp. 430–434, Apr 1987.

[5] H. Patzelt and F Arndt, "Double-plane steps in rectangular waveguides and their application for transformers, irises, and filters," *IEEE Trans Microwave Theory Tech.*, vol MTT-30, pp. 771–776, May 1982

[6] L. Carin, "Computational analysis of cascaded coaxial and circular waveguide discontinuities," Master's Thesis, Univ of Maryland, College Park, 1986.

[7] T. S. Chu and T. Itoh, "Generalized scattering matrix method for analysis of cascaded and offset microstrip step discontinuities," *IEEE Trans Microwave Theory Tech.*, vol. MTT-34, pp 280–284, Feb 1986.

[8] R. F. Harrington, *Time Harmonic Electromagnetic Fields* New York: McGraw-Hill, 1961, ch. 8.

[9] N. Marcuvitz, *Waveguide Handbook*. New York: McGraw-Hill, 1951, ch. 2.

[10] G. L. Ragan, *Microwave Transmission Circuits* New York. Dover, 1965, pp 213–214.

# A New Lock Indicator Circuit for Microwave and Millimeter-Wave Phase Locked Loops

JORDI BERENGUER I SAU, MEMBER, IEEE

***Abstract*—A new circuit useful as a lock detector in microwave PLL systems has been developed. This circuit avoids the quadrature phase detector or coherent amplitude detector commonly used as a lock indicator in PLL's, thereby reducing the microwave circuitry and components. It is based on the properties of the phase error signal coming from the phase detector; a frequency–voltage conversion is performed on it in a low-frequency (secondary) PLL, the input to which is the output of the phase detector in the main (microwave) PLL. The secondary VCO control signal gives, after a comparison, a logic level related to the lock condition in the main (microwave) PLL.**

## I. Introduction

In the development of microwave and millimeter-wave phase locked loops, where the phase detection is made at very high frequencies with conventional microwave mixers (analog multipliers), an indication of the lock condition requires the use of an additional phase detector where the VCO signal is fed through a 90° phase shifter (Fig. 1) [1]. This increases the system complex-

Manuscript received December 7, 1987; revised April 1, 1988. This work was supported by the Spanish National Commission for Science and Technology (C.A.Y.C.I.T.) under Grant 3346/83 and by the European Space Agency, with INISEL (Madrid) as main contractor.

The author is with the Dpmt. Teoria del Senyal i Comunicacions, E T S. Enginyers de Telecomunicació de Barcelona, Universitat Politècnica de Catalunya, Spain

IEEE Log Number 8822154

0018-9480/88/0900-1362$01.00 ©1988 IEEE